Towards a holistic approach to inverter-fed machine design: FEM-based PDIV prediction of complete windings

Towards a holistic approach to inverter-fed machine design: FEM-based PDIV prediction of complete windings

Jiachen Gao, *Member, IEEE*, Alberto Rumi, *Student Member, IEEE*, Yifei He, *Student Member, IEEE*, and Andrea Cavallini, *Fellow, IEEE*

***Abstract*—The Schumann inception criterion was used to predict the partial discharge inception voltage of insulation models representing both wire wound and form wound (hairpin) low voltage machines. It was found that the fitting parameter *K* (the logarithm of the critical number of electrons that define the transition from Townsend to streamer discharge) is almost independent of material parameters when dealing with a given type of insulation (e.g., turn-to-turn using round conductors or flat conductors). These numbers can be fed to software for finite element analysis to provide a worst-case estimate of the partial discharge inception voltage.**

***Index Terms*—Partial Discharges, partial discharge inception voltage, Inverter-fed machines, hairpin machines**

I. Introduction

TRACTION ELECTRIFICATION is pursued worldwide to achieve decarbonization of the transportation sector improving also the quality of the air and acoustic noise levels [1]. The backbone of electrical vehicles is the drive, made by battery, inverter, and traction motor. To save energy, inverters with a relatively high DC bus voltage (800 V) and high switching frequencies are becoming the state of the art [2]. Compared with silicone-based inverters, units based on silicon carbide (SiC) MOSFETs allow to reduce switching and conduction losses while maximizing the power density.

The advantages offered by SiC-based inverters, however, come at a cost. In the last thirty years, reliability issues of inverter-fed machines were investigated in detail and explained. Partial discharges (PD) incepted by the higher voltage stress levels due to surge reflection at the motor terminals and uneven turn voltage distribution were identified as the root cause for failure [3], [4], [5]. With SiC-based inverters, the voltage stress is expected to increase even more; besides, due to the high switching frequency, the residual life of the insulation after PD inception can be as short as minutes [6], [7]. For transport electrification, this is an important issue.

The strategy to prevent failures is to design the insulation system with a target PD inception voltage (PDIV) that is large enough to ensure that the system operates with voltage levels safely below the PDIV for a sufficiently long time. This entails (a) evaluating the voltage stress levels, and (b) defining target PDIV levels based on safety coefficients [8]. If the insulation necessary to achieve the target PDIV limits the power density of the machine, the drive can be modified to match the insulation limits by using e.g. multilevel inverters, filters, or more complex active dv/dt filtering [9], [10], [11]. After the design phase, a qualification phase consisting of accelerated life tests should be carried out, to verify that the safety coefficients were adequate to predict the effect of aging.

The whole procedure can be lengthy and costly (especially the accelerated life tests) and can delay the time-to-market of innovative solutions at the time where the situation has not stabilized yet: the automotive sector is looking forward for increasing the DC bus voltage to 1000 V or 1200 V while for the More Electrical Aircraft a *de facto* standard is not really in sight. The design phase would benefit from tools that enable the investigation of PDIV without the need of building and testing representative insulation models.

The aim of this paper is to expand a model proposed by Lusuardi *et al.* [12] for the turn-to-turn insulation of random wound motors to other geometries, including phase-to-ground and phase-to-phase insulation systems, also of hairpin machines. The approach followed to achieve this result is based on (a) the realization of insulation models as representative as possible, (b) testing PDIV experimentally, (c) modeling the geometry of the models to, (d) apply the streamer inception criterion to determine the critical number of electrons, N_{cr}, in a Townsend avalanche that cause the transition to streamer discharge. Once N_{cr} has been determined, it can be used to predict the PDIV in other, similar, geometries. In all cases, the presence of the impregnating resins was not considered, to infer the worst case in case of imperfect manufacturing.

II. Methodology

A. Test samples for wire wound motors

Two types of test samples for wire wound motors were designed: one representative of the phase-to-ground insulation, the other

of the phase-to-phase insulation; both consist of slot mockups, enameled magnet wires, and insulation films, as shown in Fig. 1. The slot mockups of the phase-to-ground insulation models were made of metal and the slot mockups of the phase-to-phase insulation models were made of PVC to completely exclude the possibility of spurious PD inception between the phases and the slot. The magnet wires used in the tests are Grade 2 wires, with an outer radius of 620 μm and enamel thickness of 30 μm. Four types of insulation films were used in the tests: Kapton polyimide film with a thickness of 50 μm, Nomex insulation paper with a thickness of 80 μm, and two Nomex-Mylar-Nomex (NMN) insulation laminates with thicknesses of 190 μm and 240 μm, respectively. Table I shows the temperature class, the thickness and relative permittivity, ε_r, of the enamel and the insulation layers at the testing temperatures. The relative permittivity of enamel and insulation layers was measured by a High-Resolution Dielectric Analyzer (Novocontrol Technologies Alpha-N). The detailed method for enamel can be found in [12].

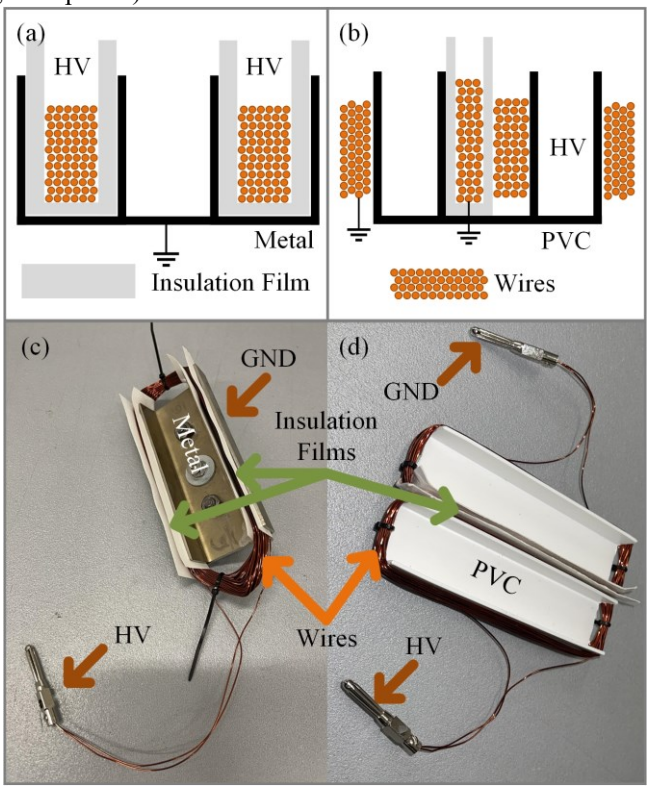

Fig. 1. Test samples for wire wound motors. (a) Schematic diagram of phase-to-ground models. (b) Schematic diagram of phase-to-phase ground. (c) Picture of a phase-to-ground model. (d) Picture of a phase-to-phase model.

The magnet wires were wound randomly by hand on the slot mockups and insulation films. Each set of magnet wires was wound at least 40 times in the phase-to-ground model and at least 20 times in the phase-to-phase model to minimize the free space within the slot. In phase-to-ground insulation models, some insulation strips (PVC or insulation paper with a thickness of 1100 μm for tests at room and high temperature, respectively) were used to press the wires to ensure close contact between the wires, the insulation films, and the slot mockups. In phase-to-phase insulation models, PVC strips were also inserted between the insulation films and the slot mockups so that the slot space was reduced, ensuring close contact between the wires and the insulation films. The head and the end of each set of magnet wires were connected by wire terminals.

TABLE I

THICKNESS AND RELATIVE PERMITTIVITY OF ENAMEL AND INSULATION FILMS OF TEST SAMPLES FOR WIRE WOUND MOTORS

Types	Thermal Class	Thickness (μm)	ε_r at 25°C	ε_r at 180°C
Enamel of Wires	220°C	30	4.55	4.59
Kapton Film	220°C	50	3.6	3.1

Nomex paper	200°C	80	1.7	1.8
NMN paper	180°C	190	2.4	2.8
NMN paper	180°C	240	2.4	2.8

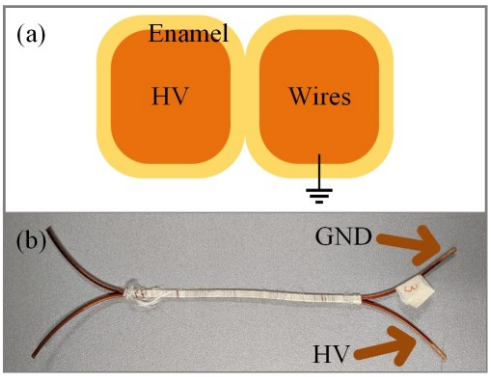

Fig. 2 Test samples for hairpin machines. (a) Schematic diagram of turn-to-turn models. (b) Picture of a turn-to-turn model.

B. Test samples for hairpin machines

Test samples for turn-to-turn PDIV in hairpin machines were made by two enameled flat wires and insulation ropes, as shown in Fig. 2. The cross-section of the wires is a 2.48×2.78 mm^2 rectangular with rounded corners of 0.8 mm radius. The wires are enameled by Polyimide-FEP (PI-FEP) with a thickness of 125 µm and 175 µm, respectively. The relative permittivity at 25°C of these enamels is 3.5. Each conductor was stripped from insulation in the terminal part for connection at the high voltage or the ground. For each different type of model, at least 3 completely fresh sets of samples were used.

C. PD Measurements

The test setup used in the PDIV measurements is shown in Fig. 3. The tests were performed in AC to achieve (1) an estimate of the PDIV not influenced by propagation phenomena within the inductive-capacitive samples, (2) the worst case for PD inception. In [13], comparative PDIV measurements performed on twisted pairs (capacitive samples, where PDIV is not influenced by propagation phenomena) using AC, repetitive square wave and surge voltages proved that AC voltages provide indeed the minimum PDIV. It is worth observing that the PDIV values provided in this way are not those of a machine, where PDIV is dependent on the turn voltage distribution through the machine design. In order to apply them, a high-frequency model of the machine is necessary to determine the electrical stress of the machine at all points of the winding.

The power supply was a 220/3000 V transformer, which can be controlled by an autotransformer at the low-voltage side. In such an arrangement, the PDIV under 50 Hz sinusoidal voltages can be measured. The voltage applied to the samples was measured by an Agilent 10076A high voltage probe (250 MHz bandwidth) and a Tektronix MDO3054 oscilloscope (2.5 GS/s sampling rate and 500 MHz bandwidth), and the peak-to-peak voltage was recorded during the test.

PD pulses were coupled by a ferrite-core high-frequency current transformer (HFCT) clamped around the DUT (Device Under Test) ground connection. The bandwidth of the HFCT exceeds 20 MHz. A coupling capacitor (1 nF) was used to improve the detection sensitivity (better than 5 pC). The signals acquired by the HFCT were transmitted to a PD detector PDBase II, which has a sampling rate of 200 MSa/s and a bandwidth of 40 MHz.

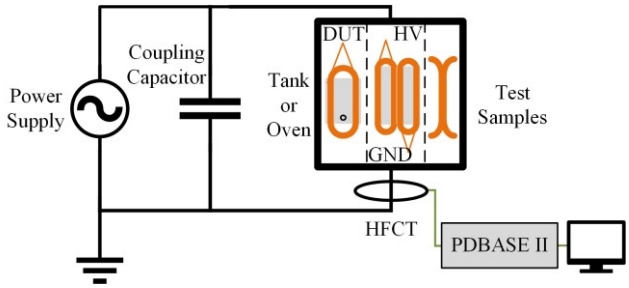

Fig. 3. Test setup

The samples were placed in a tank (room temperature) or an oven (high temperature) and connected to the high-voltage wires and ground wires. Only the phase-to-ground insulation models and flat wires models were tested in the oven at high temperatures. For both tank and oven, the peak-to-peak PDIV of the passing through wires is higher than 4 kV, larger than any PDIV value measured

during the tests.

For tests at room temperature, the measurement can be started directly after the setup. For high-temperature tests, a testing temperature of 180°C was selected as the lowest temperature class suitable for all the materials analyzed and a very common hot spot temperature used for transportation motors design. It was established to wait 20 minutes after the temperature has stabilized at 180°C in the oven to ensure that the insulation materials are isothermal. In the tests, the applied voltage was gradually increased in steps of 25 V. Furthermore, since two conditions should be met for a PD to occur: (a) the applied voltage reaches the PDIV and (b) sufficient free electrons are present in the region, it was preferred to wait 5 minutes at each step to ensure accurate PDIV measurements. For each different type of model (phase-to-ground or phase-to-phase), at least 3 completely fresh sets of samples were used; for the hairpin, 5 samples were used. For each sample, and for each condition, tests were repeated 10 times recording the minimum PDIV to single out the worst case.

III. Test Results

A. Random wound machine models

Table II shows the measured peak-to-peak values of the PDIV of random wound machine model samples, as well as the temperature (T), and the relative humidity (RT) of the air at the time each measurement was carried out. As the model samples are handmade, there are minor manufacturing differences that make the PDIV vary on a sample per sample basis for the same type of insulation models. To achieve the highest reliability in insulation design, the lowest PDIV value in each type of insulation model is taken as the reference PDIV for modeling.

Table III shows the peak value of the reference PDIV ($PDIV_{pk}$) for each type of insulation model, while the total insulation thickness and the average electric field under the PDIV are also calculated. The total insulation thickness D_t and the average electric field E_{av} are given by:

$$D_t = D_e + D_f \quad (1)$$

$$E_{av} = PDIV_{pk} / D_t \quad (2)$$

where D_e is the enamel thickness of wires. D_f is the thickness of insulation films. Note that the thickness of the enamel consists in one (D_e=30 μm) or two layers (D_e=60 μm) of wire enamel for the phase-to-ground and phase-to-phase insulation models, respectively.

Fig. 4(a) shows the dependence of the PDIV on the total insulation thickness, and Fig. 4(b) shows the average field in solid insulation at PDIV. Based on the measured PDIV data, three equations were fitted by using the least squares method for different conditions:

$$PDIV_{pk\_pp} = 0.0039 D_t + 0.7316 \quad (3)$$

$$PDIV_{pk\_pg} = 0.0029 D_t + 0.678 \quad (4)$$

$$PDIV_{pk\_pg180} = 0.0017 D_t + 0.6182 \quad (5)$$

where $PDIV_{pk\_pp}$ is the peak value of the PDIV of phase-to-phase models at room temperature. $PDIV_{pk\_pg}$ is the peak value of the PDIV of phase-to-ground models at room temperature. $PDIV_{pk\_pg180}$ is the peak value of the PDIV of phase-to-ground models at 180°C. These equations can provide simplified criteria for the design of PD-free insulation for similar conditions.

Table III and Fig. 4 show that the PDIV of insulation models at higher temperatures is lower than that at room temperature; this was expected as the temperature decreases the density of the air (favoring the discharge) and, increases the permittivity of the solid insulation (thus raising the field in the gas).

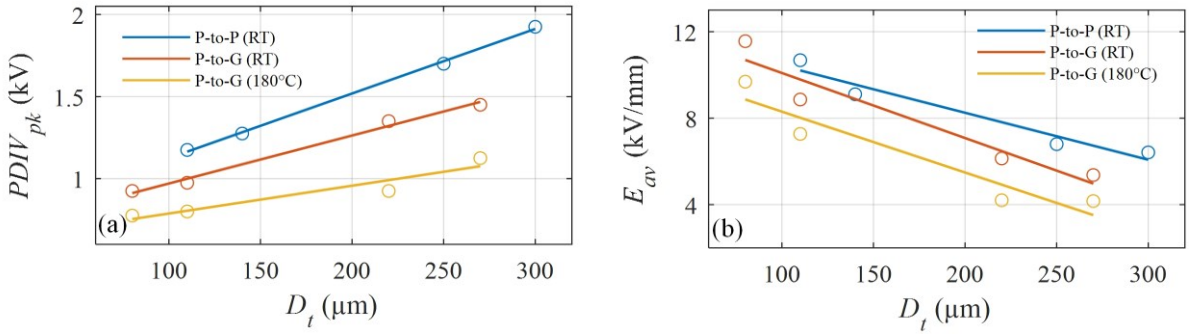

Fig. 4. Random wound machines: scatterplot of PDIV and average electric field vs insulation thickness. (a) PDIV vs insulation thickness, (b) average electric field vs insulation thickness

Table II

PDIV OF INDIVIDUAL RANDOM WOUND MACHINE MODEL SAMPLES

Model Types	Insulation Types	T (°C)	RH (%)	$PDIV_{pk}$ (kV)		
				Sample 1	Sample 2	Sample 3
Phase-to-Phase	Kapton Film (50 μm)	25	35	1.175	1.200	1.175
	Nomex paper (80 μm)	25	35	1.275	1.275	1.275
	NMN paper (190 μm)	25	35	1.700	1.700	1.700
	NMN paper (240 μm)	25	35	1.950	1.925	1.925
Phase-to-Ground	Kapton Film (50 μm)	23	40	0.950	0.925	0.950
	Nomex paper (80 μm)	23	40	1.000	0.975	0.975
	NMN paper (190 μm)	23	40	1.350	1.375	1.350
	NMN paper (240 μm)	23	40	1.525	1.450	1.450
	Kapton Film (50 μm)	180	/	0.800	0.775	0.775
	Nomex paper (80 μm)	180	/	0.800	0.800	0.800
	NMN paper (190 μm)	180	/	0.925	0.925	0.925
	NMN paper (240 μm)	180	/	1.150	1.150	1.125

Table III

MINIMUM PDIV OF RANDOM WOUND MACHINE MODEL SAMPLES

Model Types	Insulation Types	D_t (μm)	$PDIV_{pk}$ (kV)	E_{av} (kV/mm)
Phase-to-Phase (Room Temperature)	Kapton Film (50 μm)	110	1.175	10.68
	Nomex paper (80 μm)	140	1.275	9.11
	NMN paper (190 μm)	250	1.700	6.80
	NMN paper (240 μm)	300	1.925	6.42
Phase-to-Ground (Room Temperature)	Kapton Film (50 μm)	80	0.925	11.56
	Nomex paper (80 μm)	110	0.975	8.86
	NMN paper (190 μm)	220	1.35	6.14
	NMN paper (240 μm)	270	1.45	5.37
Phase-to-Ground (180°C)	Kapton Film (50 μm)	80	0.775	9.69
	Nomex paper (80 μm)	110	0.80	7.27
	NMN paper (190 μm)	220	0.925	4.20
	NMN paper (240 μm)	270	1.125	4.17

Table IV

MINIMUM PDIV OF HAIRPIN MACHINE MODEL SAMPLES

Model Types	Insulation Types	D_t (μm)	$PDIV_{pk}$ (kV)	E_{av} (kV/mm)
Turn-to-turn (Room Temperature)	PI-FEP (125 μm)	250	1.51	6.04
	PI-FEP (175 μm)	350	1.83	5.23
Turn-to-turn (180°C)	PI-FEP (125 μm)	250	1.30	5.20
	PI-FEP (175 μm)	350	1.62	4.63

B. Hairpin machine models

By using the similar method, the PDIV of the turn-to-turn insulation of hairpin machine models at room temperature was obtained, as shown in Table IV. Fig. 5 shows the dependence on the insulation thickness of the PDIV and of the average electric field in the enamel. As with the previous results of random wound machine models, the average field decreases with increasing insulation thickness. Based on the measured PDIV data, an equation is fitted as follows which can provide criteria for the design of PD-free insulation conditions:

$$PDIV_{pk\_fw} = 0.0032D_t + 0.71 \qquad (6)$$

$$PDIV_{pk\_fw180} = 0.0032D_t + 0.5 \qquad (7)$$

where $PDIV_{pk\_fw}$ is the peak value of PDIV of flat wires models at room temperature and $PDIV_{pk\_fw180}$ is the peak value of PDIV of flat wires models at 180°C.

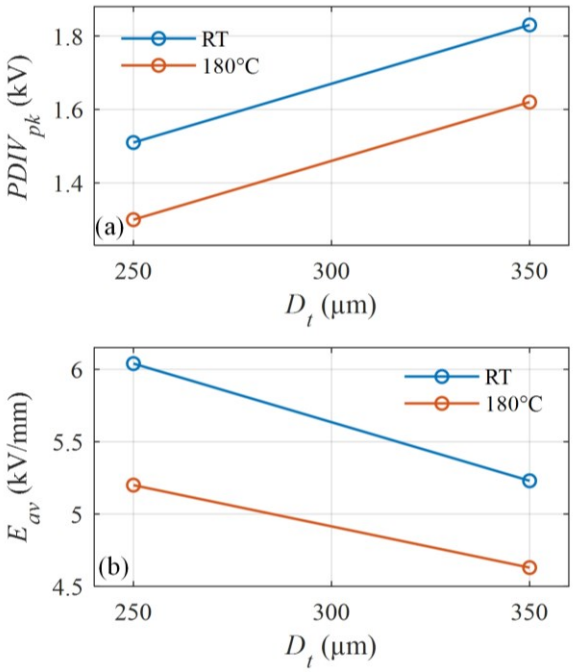

Fig. 5. Hairpin machines: scatterplot of PDIV and average electric field vs insulation thickness. (a) PDIV vs insulation thickness, (b) average electric field vs insulation thickness

IV. Prediction Model

Equations (3)-(7) obtained in the previous section can be used to some extent as criteria for insulation design. Using those equations for the PDIV prediction is desirable, due to their simplicity in the calculation. However, they are hardly applicable for different geometries, dielectrics, and operating temperatures, as different equations are found for each case. To obtain a stronger predictive tool fitting the results has been attempted with more general equations. The Dakin equation [14] is oftentimes employed due to its capability of predicting the PDIV for a large range of permittivity and thickness values. Both its classical form and a more general one (a three-parameter power law) have been used to fit the results of the hairpin insulation and phase-to-ground and phase-to-phase composite enamel and film systems. In the latter case, the permittivity of the system has been considered as the equivalent one seen from the electrodes and the thickness as the total insulation thickness. Unfortunately, neither is capable of successfully model the experimental data recorded.

This deficiency can be solved by developing an engineering model that can predict the PDIV of different conditions.

A. Model for PDIV of the twisted pairs

A prediction model for PDIV of the turn-to-turn insulation model for random wound motors (twisted pairs) was proposed by Lusuardi *et al.* [12]. The model is based on the Schumann criterion [15], which postulates that a Townsend avalanche turns into a streamer when (8) is satisfied:

$$\int_0^d \alpha_{eff}(x)\mathrm{d}x \geq K \qquad (8)$$

where α_{eff} is the effective ionization coefficient depending on the reduced electric field, and K is a dimensionless constant.

According to this criterion, Lusuardi calculated the constant K of turn-to-turn insulation models through the procedure described in [12] finding that a constant K equal to 5.98 could be used for prediction purposes. The prediction procedure was based on an iterative procedure:

a) Calculate the electric field distribution at unit voltage (see Fig. 6).
b) Start the procedure at a voltage lower than the PDIV.
c) Calculate the electric field distribution at the current voltage by linearity (using results from step (a)).
d) Calculate α_{eff}
e) Verify if (8) (with K=5.98) is satisfied for at least one electric field line.
f) If the condition in (e) is not satisfied, increase the voltage and repeat from step (c) until the voltage matches.

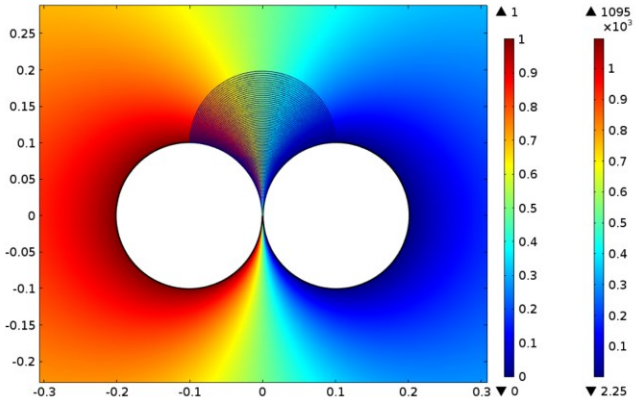

Fig. 6. Twisted pairs simulation model and electric field distribution [12].

B. K for random wound machine models and hairpin machine models

In this section, the procedure to derive the constants K is described. Compared with [12], a more efficient procedure was used here:

a) Define the geometry,
b) Set the voltage to PDIV.
c) Calculate the electric field strength across each electric field line in the gap or air region.
d) Calculate α_{eff} of every point on electric field lines by using BOLSIG+ [16], [17].
e) Calculate the left term of (8) for all field lines.
f) Select the maximum K obtained in step (e) as the K used in the streamer inception criterion (see Fig. 7).

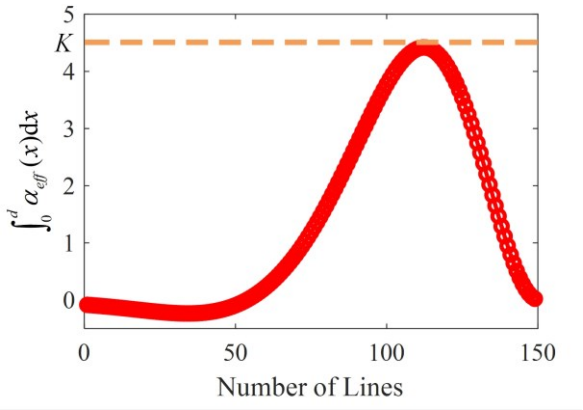

Fig. 7. Determine constant K.

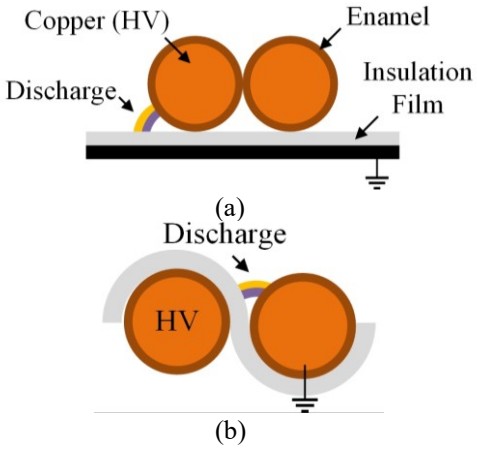

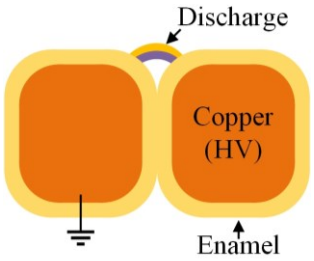

(c)

Fig. 8. Sketches of the simulation models: (a) phase-to-ground insulation, and (b) phase-to-phase insulation for random-wound machines; (c) turn-to-turn insulation for hairpin machines.

The geometries used to describe the phase-to-ground insulation, phase-to-phase insulation, and flat wires are shown in Fig. 8. The electric field distribution at 1 V was calculated as shown in Fig. 9; subsequently, the electric field strength of each field line at PDIV and the corresponding α_{eff} were calculated. Finally, the constants K of different models were determined and are reported in Table V.

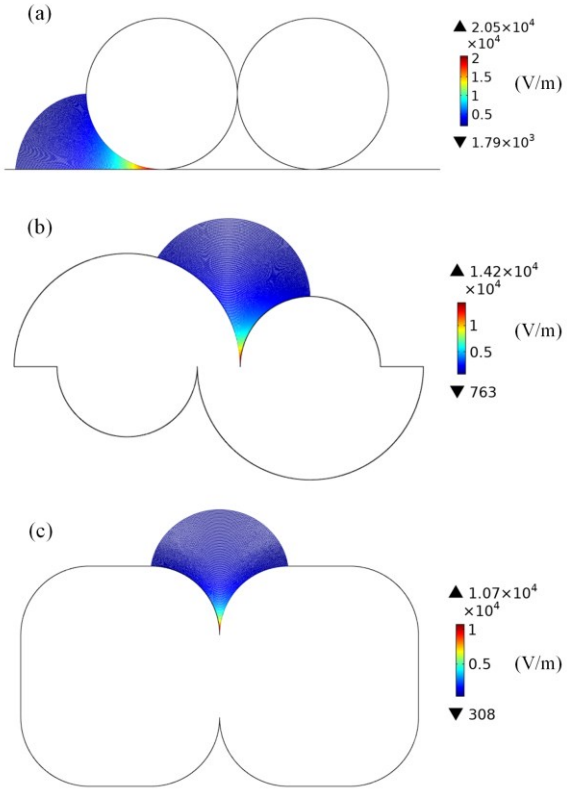

Fig. 9 Electric field distribution: (a) phase-to-ground insulation, and (b) phase-to-phase insulation for random-wound machines; (c) turn-to turn insulation for hairpin machines.

Table V

CONSTANTS K OF DIFFERENT MODELS AT ROOM TEMPERATURE

Types	Insulation Types	D_t (μm)	K
Phase-to-Phase. Random wound machines	Kapton Film (50 μm)	110	8.65
	Nomex paper (80 μm)	140	4.91
	NMN paper (190 μm)	250	4.67

	NMN paper (240 μm)	300	4.69
Phase-to-Ground. Random wound machines	Kapton Film (50 μm)	80	7.79
	Nomex paper (80 μm)	110	3.54
	NMN paper (190 μm)	220	3.51
	NMN paper (240 μm)	270	3.70
Turn-to-turn. Hairpin machines	PI-FEP (125 μm)	250	5.95
	PI-FEP (175 μm)	350	5.71

Table V shows that the constants K in phase-to-phase and phase-to-ground insulation models display relatively large differences from K=5.98 as determined by Lusuardi *et al.* [12]. If K=5.98 is still used as the criterion in (8), the prediction results will be affected by large errors.

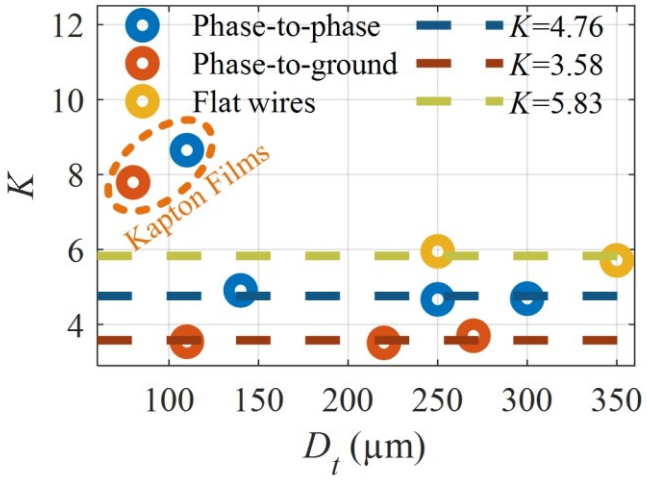

Fig. 10. Constants K of phase-to-phase, phase-to-ground, and flat wires models.

Fig. 10 shows the constants K of phase-to-phase, phase-to-ground, and flat wires models with different total thicknesses. The constants K of phase-to-phase and phase-to-ground insulation models made of Nomex papers and NMN papers, and flat wires models are independent of the insulation thickness. The constants K of phase-to-phase and phase-to-ground insulation models made of Kapton films are much larger than those of other models. This may be due to the features of the Kapton film, which is thin and soft: both features can lead to significant differences between the insulation models and the geometries used for the simulations. Using the K values adopted for the other cases might be considered a conservative choice (i.e., the simulated PDIV values will be lower).

The average values of the constants K of phase-to-phase and phase-to-ground insulation models with insulation papers, and flat wires, were $K_{average}$=4.76 for phase-to-phase insulation, $K_{average}$=3.58 for phase-to-ground insulation, $K_{average}$=5.83 for flat wires models. These values can be used to evaluate the likelihood of PD inception in the insulation using the prediction model described in Section IV-A.

C. Application of Prediction Model

The accuracy of the prediction model was estimated for the room temperature test conditions, calculating the deviance from the experimental data. Additionally, to test the capability of the model to predict the PDIV in different conditions, predictions of the PDIV of phase-to-ground insulation models and flat wires models at high temperatures (180°C) were also carried out.

To achieve predictions for environments with different temperatures, the influence of temperature on the calculations needs to be considered. There are two parts of the prediction process that are affected by the ambient temperature. The first part is that in the electric field distribution calculation, the ambient temperature might change the relative permittivity of the materials. This can be accounted for by performing the dielectric spectroscopy at the desired temperature and setting the materials permittivity in the finite element method (FEM) software accordingly (note that, for resins above the glass transition temperature, this can be difficult [18]). In this case, the permittivity of the laminates at 180°C was measured, as explained in Section II. The permittivity of the enamel was assumed to be equal to that at room temperature, as the glass transition temperature of the polyamide-imide enamel is normally much larger than 180°C and therefore the permittivity is not expected to change remarkably.

The second part is that the ambient temperature changes the number of particles per unit volume N of the air, and therefore the

reduced electric field which affects the effective ionization coefficient α_{eff}. The number of particles per unit volume N can be determined using the ideal gas law:

$$pV = Nk_bT \quad (9)$$

where p is the absolute pressure of the gas, V is the volume, k_b is the Boltzman constant, and T is the absolute temperature. Combining the number of particles per unit volume with the calculated electric field distribution, the effective ionization coefficient α_{eff} can be derived using Bolsig+ [17]. By considering the above two parts, prediction calculations for different temperature environments can be realized.

The impact from thermal expansion can be ruled out, as negligible variations in the thicknesses are estimated in the temperature range considering the thermal expansion coefficient of the materials involved [18].

Table VI shows the results of the predictions. It can be seen that the predicted results agree well with the test data at room temperature with a maximum error of 1.48%. There is also good accuracy in high-temperature environments with a maximum error of 10.49%. In summary, it can be stated that the prediction model presented in this paper has good accuracy and applicability and can contribute to insulation design for wire wound motors and hairpin machines.

V. Conclusion

This paper proposed a prediction model for the design of the electrical insulation of random wound and hairpin machines. The use of simplified fitting formulas can provide for single materials and limited geometries a good prediction of PDIV values. Unfortunately, the approach is not useful in the design phase, as materials in that condition can be tested directly for their tentative design sizing and operative condition. A more general prediction model based on the electric field simulation and streamer inception criterion was proposed based on experimental data. Interestingly, no dependence on the geometry/material properties of the constant used for the streamer inception criterion was found, with different values obtained for the three geometries analyzed. On one side the result is disappointing as prediction models remain bounded to fitting parameters (in this case, the constant K) which depend on the geometry of the insulations. On the other hand, a single K parameter value can possibly be sufficient for any of the geometries across a vast range of materials and sizes.

The model provides an agreement with the experimental PDIV results with a maximal error of 1.48% at room temperature. Attempting prediction of experimental results obtained in high-temperature environments it estimates the PDIV with an error of 10.49% proving a good accuracy and applicability.

It is noteworthy that the proposed model was based on the experimental data of air-cooled machines. Therefore, for machines using direct cooling methods, such as using water cooling, oil cooling, or using other cooling fluids, the validity of this prediction model requires further validation with more experimental data.

The findings can contribute to insulation design for wire wound motors and hairpin machines.

Table VI.
Predicted $PDIV_{pk}$ vs Measured $PDIV_{pk}$

Types	Insulation Layer	D_t (μm)	Predicted $PDIV_{pk}$ (kV)	Measured $PDIV_{pk}$ (kV)	Error (%)
Phase-to-Phase Ran. wound machines (Room Temperature)	Nomex paper (80 μm)	140	1.26	1.275	-1.18
	NMN paper (190 μm)	250	1.72	1.70	1.18
	NMN paper (240 μm)	300	1.94	1.925	0.78
Phase-to-Ground Ran. wound machines (Room Temperature)	Nomex paper (80 μm)	110	0.98	0.975	0.51
	NMN paper (190 μm)	220	1.37	1.35	1.48
	NMN paper (240 μm)	270	1.44	1.45	-0.69
Turn-to-turn Hairpin machines (Room Temperature)	Polyimide-FEP (125 μm)	250	1.50	1.51	-0.66
	Polyimide-FEP (175 μm)	350	1.85	1.83	1.09
Phase-to-Ground Ran. wound machines (180°C)	Nomex paper (80 μm)	110	0.74	0.80	-7.50
	NMN paper (190 μm)	220	0.92	0.925	-0.54
	NMN paper (240 μm)	270	1.03	1.125	-8.44
Turn-to-turn Hairpin machines (180°C)	Polyimide-FEP (125 μm)	250	1.19	1.30	-8.46
	Polyimide-FEP (175 μm)	350	1.45	1.62	-10.49

REFERENCES

[1] C Li, *et al*. "Insulating materials for realising carbon neutrality: Opportunities, remaining issues and challenges," *High Voltage*, vol. 7, no. 4, pp. 610-632, Aug. 2022, doi: 10.1049/hve2.12232.

[2] C. Jung, "Power Up with 800-V Systems: The benefits of upgrading voltage power for battery-electric passenger vehicles," *IEEE Electrification Mag.*, vol. 5, no. 1, pp. 53–58, Mar. 2017, doi: 10.1109/MELE.2016.2644560.

[3] G. Stone, S. Campbell, and S. Tetreault, "Inverter-fed drives: which motor stators are at risk?," *IEEE Ind. Appl. Mag.*, vol. 6, no. 5, pp. 17–22, Sep. 2000, doi: 10.1109/2943.863631.

[4] M. Kaufhold, H. Aninger, M. Berth, J. Speck, and M. Eberhardt, "Electrical stress and failure mechanism of the winding insulation in PWM-inverter-fed low-voltage induction motors," *IEEE Trans. Ind. Electron.*, vol. 47, no. 2, pp. 396–402, Apr. 2000, doi: 10.1109/41.836355.

[5] Weijun Yin, "Failure mechanism of winding insulations in inverter-fed motors," *IEEE Electr. Insul. Mag.*, vol. 13, no. 6, pp. 18–23, Nov. 1997, doi: 10.1109/57.637150.

[6] L. Lusuardi, A. Rumi, A. Cavallini, P. Wang, and T. Han, "Can Low Voltage Inverter-Fed Induction Motors Be Designed Allowing Partial Discharge Activity?," in *2019 IEEE Electrical Insulation Conference (EIC)*, Jun. 2019, pp. 79–82. doi: 10.1109/EIC43217.2019.9046548.

[7] A. Rumi, J. G. Marinelli, D. Barater, A. Cavallini, and P. Seri, "The Challenges of Reliable Dielectrics in Modern Aerospace Applications: The Hazard of Corona Resistant Materials," *IEEE Trans. Transp. Electrification*, vol. 8, no. 4, pp. 4646–4653, Dec. 2022, doi: 10.1109/TTE.2022.3191064.

[8] IEC Std. 60034-18-41, *Rotating electrical machines - Part 18-41: Partial discharge free electrical insulation systems (Type I) used in rotating electrical machines fed from voltage converters - Qualification and quality control tests*. 2019.

[9] S. Lee and K. Nam, "An overvoltage suppression scheme for AC motor drives using a half DC-link voltage level at each PWM transition," *IEEE Trans. Ind. Electron.*, vol. 49, no. 3, pp. 549–557, Jun. 2002, doi: 10.1109/TIE.2002.1005379.

[10] T. Fuchslueger, H. Ertl, and M. A. Vogelsberger, "Reducing dv/dt of Motor Inverters by Staggered-Edge Switching of Multiple Parallel SiC Half-Bridge Cells," in *PCIM Europe 2017; International Exhibition and Conference for Power Electronics, Intelligent Motion, Renewable Energy and Energy Management*, May 2017, pp. 1–8.

[11] A. Rumi, L. Lusuardi, A. Cavallini, M. Pastura, D. Barater, and S. Nuzzo, "Partial Discharges in Electrical Machines for the More Electrical Aircraft. Part III: Preventing Partial Discharges," *IEEE Access*, vol. 9, pp. 30113–30123, 2021, doi: 10.1109/ACCESS.2021.3058090.

[12] L. Lusuardi, A. Cavallini, M. G. de la Calle, J. M. Martínez-Tarifa, and G. Robles, "Insulation design of low voltage electrical motors fed by PWM inverters," *IEEE Electr. Insul. Mag.*, vol. 35, no. 3, pp. 7–15, May 2019, doi: 10.1109/MEI.2019.8689431.

[13] L. Lusuardi, A. Cavallini, A. Caprara, F. Bardelli and A. Cattazzo, "The Impact of Test Voltage Waveform in Determining the Repetitive Partial Discharge Inception Voltage of Type I Turn/Turn Insulation Used in Inverter-Fed Induction Motors," 2018 IEEE Electrical Insulation Conference (EIC), San Antonio, TX, USA, 2018, pp. 478-481, doi: 10.1109/EIC.2018.8481018.

[14] T. W. Dakin, H. M. Philofsky and W. C. Divens, "Effect of electric discharges on the breakdown of solid insulation," in *Electrical Engineering*, vol. 73, no. 9, pp. 812-817, Sept. 1954, doi: 10.1109/EE.1954.6438979.

[15] W. O. Schumann, "Über das Minimum der Durchbruchfeldstärke bei Kugelelektroden," *Arch Elektrotech. Berl*, vol. 12, pp. 593–608, 1923.

[16] G. J. M. Hagelaar and L. C. Pitchford, "Solving the Boltzmann equation to obtain electron transport coefficients and rate coefficients for fluid models," *Plasma Sources Sci Technol*, vol. 14, no. 4, pp. 722–733, 2005.

[17] "BOLSIG+ | Electron Boltzmann equation solver." http://www.bolsig.laplace.univ-tlse.fr/ (accessed Sep. 10, 2021).

[18] A. Rumi, J. Marinelli, and A. Cavallini, "Dielectric Characterization of Impregnating Varnishes for Inverter-Fed Motors," in *2022 IEEE 4th International Conference on Dielectrics (ICD)*, Jul. 2022, pp. 389–392. doi: 10.1109/ICD53806.2022.9863563.

Jiachen Gao (Member, IEEE) was born in Dalian, Liaoning, China, in 1995. He received the B.E. degree in electrical engineering and its automation, the M. E. and the Ph.D. degrees in electrical engineering from Wuhan University, China, in 2017, 2019, and 2022, respectively, and the Ph.D. degree in biomedical, electrical and systems engineering from the University of Bologna, Italy, in 2022.

He is currently an assistant professor with the College of Electrical and Information Engineering, Hunan University. His current research interests include discharges in long air gaps and the reliability of inverter-fed motors.

Alberto Rumi (Student Member, IEEE) is currently pursuing a Ph.D. in Electrical Engineering at the University of Bologna, where he also graduated with honours (B.Sc. 2016 and M.Sc. 2019). His research activity focuses on the characterization of electrical insulating materials for low voltage rotating machines fed by converters based on wide-bandgap devices. His research interests include diagnosis by partial discharge analysis, polymers ageing mechanisms and the reliability of the inverter-motor chain in aeronautical and automotive fields.

Yifei He (Student member, IEEE) was born in Shaanxi, China, in 1995. He received the B.S. degree in electrical engineering from Xi'an Jiaotong University, Xi'an, in 2017. Now, he is a Ph.D. student in the Department of Electrical Engineering of Xi'an Jiaotong University. His research interests are in space charge properties and the mechanism of charge transport.

Andrea Cavallini (Fellow, IEEE) is full professor at the University of Bologna, Italy. He was a co-Founder of spinoff company Techimp HQ Spa, Italy. He is the author or a coauthor of more than 280 international articles. He holds 16 international patents. His research interests include the diagnosis of insulation systems by partial discharge analysis, reliability of electrical systems, and artificial intelligence. Dr. Cavallini is a member of International Electrotechnical Commission (IEC) TC 2/MT 10 and a Project Leader of IEC 60034-18-41 Ed. 2